Structural analysis of a 'Foiling Moth' sailing dinghy hydrofoil

R. Ponte, L. Sutherland & Y. Garbatov
Centre for Marine Technology and Engineering (CENTEC), Instituto Superior Técnico, University of Lisbon, Portugal

ABSTRACT: An ABAQUS finite element analysis (FEA) of the main strut of a foiling Moth high-performance sailing dinghy has been developed and validated experimentally with full-scale mechanical tests representative of the sailing condition. Agreement between experimental and numerical results was excellent, solely by using engineering-based choices for both the internal structural arrangement and the pertinent experimentally based library material properties, i.e., without the need for 'calibration' of the model parameters. This gives a high level of confidence in the validation of the FE model. The FE model is the first stage of the ongoing development of a full fluid-structure interaction (FSI) tool, which will be obtained by combining the FEA with a computational fluid dynamics (CFD) model. This FSI will be a valuable and economic tool in facilitating evaluations of different foil appendage lay-up and fabrication methods designed to optimize the sailing performance.

1 INTRODUCTION

The International Moth is a single-handed extremely lightweight 'foiling' sailing dinghy, and this study specifically considers the commercially available 'Voodoo' Moths as manufactured at Trimarine Compósitos Lda, https://www.trimarine.com/en/home-en/ (Figure 1).

Figure 1 'Voodoo' Foiling Moth at Cascais © Rui Brites

The craft has an overall length of 3.335m, a beam at the waterline of just 0.3m, with large 'wings' to keep the sailor's righting moment sufficiently outboard (and giving the class its name), a sail area of 8 m² and a fully-rigged weight as little as 26 kg (Banks et al., 2016, Findlay & Turnock, 2008, IMCA Rules, 2017). It is a development class boat and follows open class rules (IMCA Rules, 2017). In recent years, the development of lifting carbon fibre reinforced plastic (CFRP) horizontal hydrofoils (Figure 2) at the bottom of the dagger-board and rudder blade have enabled it to fly above the water surface, dramatically reducing drag and increasing speeds up to 35 knots. The large power to weight ratio allows the foils to lift the hull up out the water with just 5 knots of true wind.

Figure 2 Main (dagger-board, top) and rudder (bottom) foils (Allen, 2017)

An active control mechanism is required to control the 'ride height' above the water over a range of speeds, and this is achieved using a 'wand' mounted at the bow (Figure 3) that controls the camber with a moveable flap on the trailing edge of the forward hydrofoil via a cam and pushrod system. The angle of attack of the aft rudder-mounted hydrofoil can be manually adjusted while sailing (using a twist-grip tiller extension (Figure 3) connected to a worm gear system) thus controlling the pitch of the boat and hence fine-tuning the ride height.

The dagger-board is referred to as the 'main strut' (Figure 3) since its main function is to support the weight of, and sailing loads produced by, the boat, rig, and main foil; it has only a very small, wetted surface when foiling and hence provides correspondingly very small hydrodynamic forces. Hence, as shown in Figure 4, the up-wind force required to counter the sail downwind force ($F_{S,H}$) must be achieved by heeling the moth, and hence the foils, to windward, thus rotating the 'lift' force (F_F) and producing an upwind force component ($F_{F,H}$).

Figure 3 Parts of a foiling moth © Rui Brites (adapted)

The sailor dynamically maintains the equilibrium of the various heeling moments due to the lateral forces shown in Figure 4 mainly by adjusting their body weight position laterally and by controlling the power of the rig.

Hence, since the main foil is providing both lifting and upwind forces at the end of the 1.04 m long main strut, the strut is extremely highly loaded. The fact that the aft rudder foil provides little of the lift required exacerbates the loadings on the main strut.

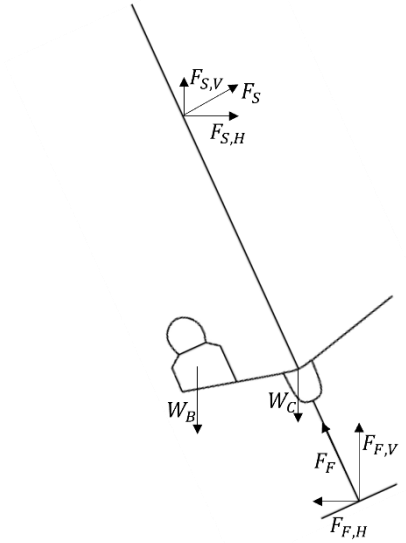

Figure 4 Heel angle and lateral foiling forces, F, and weights, W. Subscripts: F = foil, S = Sail, C = Craft, B = Body, H = Horizontal, V = Vertical

When foiling, the aft foil operates at very low to negative lift loadings, helping the sailor's bodyweight pull down the stern in opposition to the bow down pitch moment set up by the forward force of the sail together with the foil drag (Findlay & Turnock, 2008) (Figure 5).

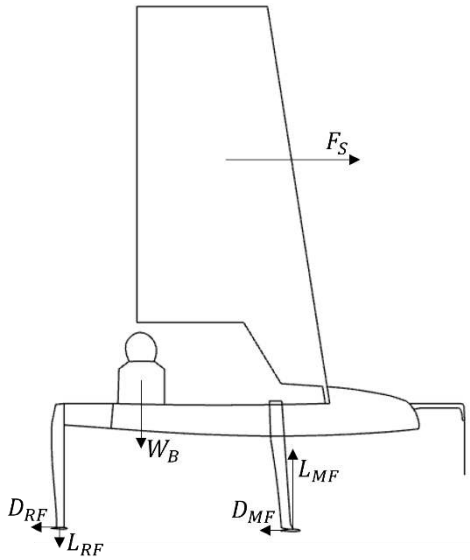

Figure 4.
Figure 5 Fore-Aft foiling forces, lift, L, and drag D, forces, subscripts: MF = main foil and RF = rudder foil

The structural performance of the main strut is thus of the utmost interest, and therefore a finite element analysis is developed here to enable both comparisons with existing, empirically proven (i.e., well-sailed) designs, and to help refine and develop existing and new designs. This FE model will also serve as the first stage in the ongoing development of a full fluid-structure interaction tool for the design and optimization of these hydrofoils.

This work details sequentially the strut geometry, materials, and construction, and then the FE model and its validation via mechanical tests in the following sections.

2 GEOMETRY, MATERIALS AND CONSTRUCTION

Trimarine Compósitos Lda supplied the 3D Step file (.stp) geometrical model of the main strut and hydrofoil assembly (constructed for fabrication of the moulds). After importation to Rhino3D (McNeel et al, 2010) (Figure 6), the surfaces were refined, and any small inconsistencies were corrected to avoid errors in the ABAQUS (ABAQUS, 2021) FE modelling.

Since the focus of this particular paper is the main strut, the mail foil was not modelled in the FEA. In addition, to save resources, since the main strut acts as a cantilever extending from the hull bottom, the part of the strut that sits inside the dagger-board case in the hull was also not included in the FEA.

Figure 6 Main strut and foil (shown rotated by 90º).

Fabrication of the main strut uses a vacuum-assisted hand layup method. First, a skin-coat of resin is applied to each half of the mould with a brush and then the reinforcements are applied ply-by-ply. Manual consolidation and compaction with metal rollers and application of more resin as needed occurs between each ply, until both port and starboard entire laminates are laid down (see Figure 7). Different areas of the foil have different numbers, types, and alignments of reinforcement fibres, following the (commercially sensitive) lay-up 'schedule'.

Once the laminates have been laid down, the wet parts are covered with peel ply - a perforated polymer film to give a textured surface finish for subsequent bonding and to allow easy removal of the subsequent disposable layers whilst enabling the excess resin to pass through it. Then this is covered with a layer of breather cloth - a loose felt material to ensure even pressure distribution and to absorb removed excess resin. Finally, the airtight vacuum bags are applied and sealed around the port and starboard sides to the mould flanges using 'tacky tape' (a sticky putty type material providing a good air seal). The vacuum is then applied with a pump, further consolidating the laminate, and removing any excess resin. The vacuum is held and maintained until both sides are cured.

On removal of the peel ply, breather and vacuum bag from both half-moulds, a shaped polymer foam 'half-core' is applied and glued to the interior face of both laminates with a structural adhesive, which also fills any smaller voids where there is no core (Figure 8).

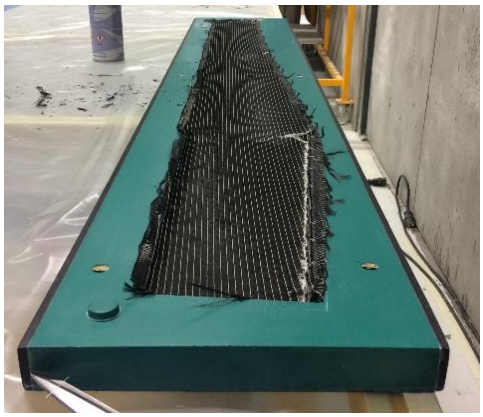

Figure 7 Laminate ply layup (before vacuum bag application).

When the core adhesive has cured, the upper surfaces of both sides are sanded to ensure flat and well-keyed upper surfaces, which are then bonded together using structural adhesive. The two female mould flanges are bolted together until the adhesive cures to give a single part, which is then removed from the mould (Figure 9). The moulding flashings are then removed, and the strut is finished by hand.

Figure 8 Core and structural adhesive application.

Figure 9 Main strut on removal from the mould.

The carbon fibre reinforcements used are 200 g/m^2 twill woven fabric, 400 g/m^2 biaxial fabric, 340 g/m^2 ultra-high modulus (UHM) and 300 g/m^2 standard modulus (SM) UD (unidirectional) reinforcements. The matrix resin is Gurit Ampreg™ 31 (Gurit, 2021) epoxy with standard hardener (Gurit, 2021), the core is Gurit Corecell® M200 structural SAN polymer foam (Gurit, 2019a) and the structural adhesive is Spabond™ 345 (Gurit, 2019b).

The exact details of the layup used are commercially sensitive, but there are a total of 36 plies on each side of the foil, of which 3% are woven fabric, 42% are UD and 55% are biaxial fabric +45º/-45º (the latter of which gives torsion control and strength). The width and length of the various plies vary from 30 to 150 and from 100 to 1450 mm in width and length, respectively.

The tenon and surrounding area on the main strut (which is screwed and bonded into a mortise on the main foil) is heavily reinforced since this is a highly stressed joint.

3 FINITE ELEMENT MODEL

ABAQUS 2021 software (ABAQUS, 2021) was used for the FEA due to its ability to model composite materials and its compatibility with the CFD software, Star-CCM+ (Siemens Simcenter Star-CCM+, 2020), which will be required for the FSI analyses to be completed.

The general-purpose, 8-node, hexahedral, first-order, reduced-integration, continuum shell element, SC8R was used since it can both precisely model the complex fin geometry and reduce computational expenses. Further, this element accounts for finite membrane strains, arbitrary large rotation, and allows for

changes in thickness, making it suitable for this large strain/displacement analysis.

The continuum shell SC8R element was preferred over conventional shell elements since the latter would not be capable of defining the inner areas of core and structural adhesive (Sutherland et al., 2021).

The SC8R element requires hexahedral meshing, and since it is a first-order reduced-integration element, the mesh must be sufficiently fine to avoid 'hour-glassing'. Hence, a nominal mesh size of 5 mm, resulting in a mesh of 26390 elements was used (Figure 10).

Figure 10 FE mesh.

With a 1/ (number of elements) parameter of 3.79×10^{-5}, this is a sufficiently fine mesh according to previous comparable studies (Giovannetti 2017, Brito 2021).

Given the variation of laminate layup over the foil area, it was necessary to divide the geometry up into partitions within each of which the layup is constant.

Figure 11 Main strut FE partitions.

The ply layup of each partition was defined as an ABAQUS 'composite set', allowing the laminate mesh to subdivide through the laminate thickness without the need to partition the laminate in this direction. This facilitates greatly any changes that need to be made to the layup, which will be an important advantage when using the completed tool to investigate the performance of alternative lay-ups.

Cured ply thicknesses, t mm, were calculated from the fiber volume fraction, V_F, fibre density, ρ_F, g/cm^3 and reinforcement areal weight, W_F, g/m^2, using equation (1) (Gurit, 2017) to give the values in Table 1.

$$t = \frac{W_F}{\rho_F \, FVF \, 1000} \tag{1}$$

Table 1 Calculated ply thicknesses.

Carbon Fibre	Density, g/cm^3	Thickness, mm
200 g/m^2 Woven	1.451	0.251
400 g/m^2 Bi-axial	1.518	0.479
340 g/m^2 UHM UD	1.540	0.368
340 g/m^2 SM UD	1.490	0.366

Fibre densities were obtained from the suppliers' data sheets (Toray 2018a, b, Mitsubishi). The values provided by Trimarine Compósitos Lda of 0.55 and 0.60 for the fibre volume fractions of the woven and UD reinforced plies, respectively, correspond with typical literature values for vacuum-assisted hand layup (Sleight, 1985).

Once the thickness of the skin laminates of both sides of the foil had been modelled, the areas between them that are filled with foam core during fabrication were identified and modelled as core, accordingly. Any other central, smaller central voids around the edges of the cored areas were modelled as containing structural adhesive – again reflecting the actual manufacturing process.

The material properties for the laminated plies were obtained from the (experimentally based) ANSYS material library (ANSYS© 2020 R2, 2020). The library materials selected were not only those fabricated using the same vacuum-assisted hand layup method but were also of the same fibre volume fractions as those used in the strut.

Table 2 FEA ply material properties.

Woven	Bi-axial	UHM UD	SM UD	
E_x , MPa	59200	91820	209000	121000
E_y , MPa	59200	91820	9450	8600
E_z , MPa	7500	90000	9450	8600
ν_x	0.04	0.05	0.27	0.27
ν_y	0.3	0.3	0.4	0.4
ν_z	0.3	0.3	0.27	0.27
G_{xy} , MPa	3300	3600	5500	4700
G_{yz} , MPa	2700	3000	3900	3100
G_{xz} , MPa	2700	3000	5500	4700

The core material properties used were - Young's moduli, E_x and E_y: 210 MPa, Poisson's ratio, ν_x: 0.33, and shear modulus, G_{xy}: 0.098 MPa (Gurit, 2019a). A bulk modulus, E, of 3007 MPa, and Poison's ratio, ν, of 0.38 were assumed for the structural adhesive (Pham & Mohareb 2015).

4 MECHANICAL TESTS AND FEA VALIDATION

It is imperative to validate any finite element model against real physical experimental test data if any confidence in its results is to be assumed. To achieve this, mechanical tests on an actual main strut were carried out. A simple fully clamped cantilever set up with a point load close to the strut tip was used since it is sufficiently representative of actual sailing loadings and is simple enough to ensure that reliable and accurate experimental data could be obtained.

The mechanical tests were completed using a calibrated, computer-controlled servo-hydraulic machine, which recorded the applied force and displacement at the loading point with time (Figure 12).

Figure 12 Experimental setup & maximum deflection.

The load was applied via a hemispherical steel load cell attachment at 20 mm from the strut tip (i.e., 1060 mm from the clamp) and 70 mm from the trailing edge. Tests were carried out under ramped displacement control at 0.1 mm/s. Tests were stopped at a maximum load of 600 N, which gave a maximum displacement sufficiently large to enable validation of the FEM, but with little risk of breaking the strut. Six repetitions of the test were made to give an estimate of the experimental error. After the tests with the load on the port side of the strut were completed, the strut was turned over and the same test setup was used to give results for the starboard side.

Signals were sampled at 50 Hz and electrical noise in the raw data was removed using a simple moving average, which did not remove any features of the linear behaviour seen.

The representative example of the experimental test results shown in Figure 13 show extremely linear behaviour, as would be expected for these vacuum-bagged carbon fibre materials, and the fact that it continues up to the maximum load-tested indicates that no significant damage to the strut occurred.

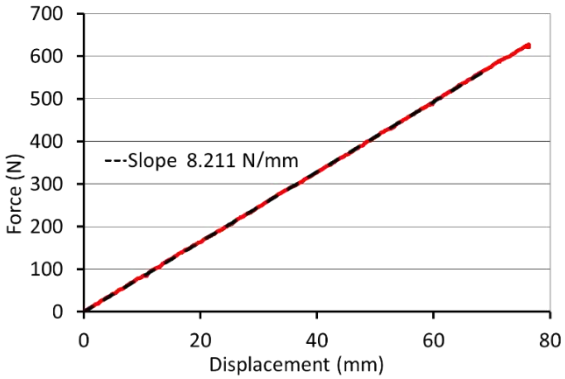

Figure 13 Experimental results (Portside test #2).

The full set of results is plotted in Figure 14. The fact that the six red lines corresponding to the tests on the port side are indistinguishable shows that a high level of repeatability has been achieved and reinforces the inference made above that no damage was incurred by the strut. The same conclusions can also be made for the green lines representing the tests on the starboard side.

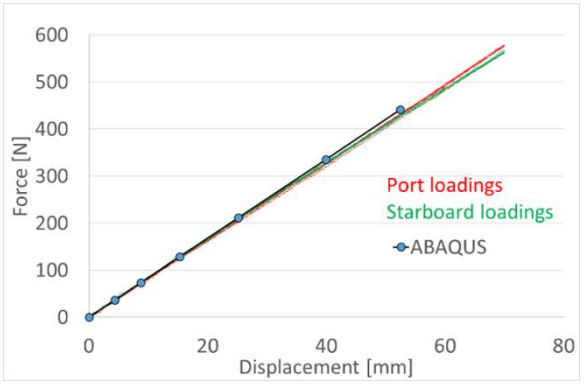

Figure 14 Experimental and FEA results.

In addition, the strut has little asymmetry since green and red (starboard and port loaded) plots are very nearly coincident. The experimental cantilever stiffness values presented in Table 2 confirm these observations.

Table 3 Experimental cantilever stiffness values.

Test Replication	Stiffness (N/mm)	
	Port	Starboard
1	8.00	8.07
2	8.21	8.02
3	8.24	8.04
4	8.23	8.02
5	8.23	8.01
6	8.21	8.00
Average	8.19	8.03
Coeff. of Variation	1.1%	0.3%
Strut Average	8.11	
ABAQUS	8.42	

To validate the FE model the mechanical test setup was replicated with the same clamping at the hull end of the strut and single point load application position (Figure 15)

Figure 15 FEA validation setup.

As for the experimental tests, an increasing ramp load was applied whilst the force and calculated displacements at the load point were recorded. As can be seen in both Figure 14 and Table 2, the agreement between experimental and numeric results is excellent, validating the FEA for this type of loading, which is representative of the sailing condition. It is important to note that the agreement between the FE analyses and experimental results has been obtained solely by both ensuring that the structural model is representative of the details of the layup and manufacturing process, and by using experimentally obtained library material

properties of equivalent materials. In other words, no 'calibration' (i.e., fitting of the FE model to the experimental data via adjustment of the material properties) was required. This gives a high degree of confidence that the FE model is representative of the real, physical case.

5 CONCLUSIONS

The 'main strut' (dagger-board) supports the majority of the sailing loads of a 'foiling' Moth sailing dinghy. Hence, an ABAQUS finite element analysis of this strut has been carried out and validated experimentally with full-scale mechanical tests representative of the sailing condition.

Agreement between experimental and numerical results was excellent, solely by using engineering-based choices for both the internal structural arrangement and the pertinent experimentally based library material properties, i.e., without the need for 'calibration' of the model. This gives high confidence in the validation of the FE model.

The FE model is the first stage of the planned development of a full fluid-structure interaction tool. Extension of the FE model to encompass the full main hydrofoil assembly (i.e., vertical main strut plus horizontal main hydrofoil 'wing') is now underway as is the development of the corresponding computational fluid dynamics analysis using Star-CCM+ (where little of the main strut is actually submerged and hence producing hydrodynamic loads). The full FSI model will be obtained by combining the FEA and CFD models through the Simulia Co-Simulation engine (Co-Simulation Engine, 2021). The FSI will be a valuable and economic tool in facilitating evaluations of different foil appendage lay-up and fabrication methods designed to optimize the sailing performance.

6 REFERENCES

ABAQUS. 2021. Abaqus Unified FEA-3DEXPERIENCE R2021. Dassault Systèmes, Rhode Island.

Allen, C. 2017. Voodoo Boats. URL http://voodooboats.com. Accessed 25/01/2022.

ANSYS© 2020 R2. 2020. ANSYS Inc, Cannonsburg, PA, USA.

Banks, J., Marimon Giovannetti, L., Taylor, J.C., Turnock S.R. 2016. Assessing Human-Fluid-Structure Interaction for the International Moth. *Procedia Engineering* 147: 311-316.

Barbero, E. 2013. Finite Element Analysis of Composite Materials Using Abaqus™. Boca Raton: CRC Press.

Brito, M. 2021. An integrated FSI analysis of a windsurf fin. MSc thesis, Instituto Superior Técnico, Lisbon, Portugal.

Co-Simulation Engine, 2021. Dassault Systems Simulia Corp, Rhode Island.

Findlay, M., Turnock, S. Investigation sailing styles and boat set-up on the performance of a hydro foiling moth dinghy. *20th International HISWA Symposium on Yacht Design and Yacht Construction,* Amsterdam, Netherlands, 17-18 November, 2008, pp 38 -52.

International Moth Class Rules (IMCA). 2017.

Giovannetti, L. 2017 Fluid-structure interaction testing, modelling and development of passive adaptive composite foils. PhD Thesis, University of Southampton, Southampton, UK.

Gurit. 2017. Guide to Composites.

Gurit. 2019a. Corecell™ M: The marine foam. M-10-119 datasheet.

Gurit. 2019b. Spabond™ 345 Epoxy adhesive system. PDS-Spabond345-16-1119 datasheet.

Gurit. 2021. Ampreg™31 Epoxy wet lamination system, PDS-AMPREG-31-6-0721 datasheet.

McNeel, R., '& others'. 2010. Rhinoceros 3D, Version 6.0. Robert McNeel & Associates, Seattle, WA.

Mitsubishi. High modulus carbon. UD-330G-WBI datasheet.

Siemens Simcenter STAR-CCM+. 2019. Siemens Industries Digital Software, Munich, Germany.

Sleight, S. 1985. Modern Boat Building Materials, Conway Maritime Press Ltd, London, UK.

Sutherland, L.S., Cardoso de Brito, M., Chaves Pereira, J., Benson, S. 2022. Fluid-structure interaction analyses of a composite windsurf fin. *MARTECH 6th International Conference on Maritime Technology and Engineering,* Lisbon, Portugal.

Toray. 2018a. T300 Standard Modulus Carbon Fiber. T300-Technical-Data-Sheet-1.

Toray. 2018b. T700S Standard Modulus Carbon Fiber. T700S-Technical-Data-Sheet-1.

Van Pham, P., Mohareb, M. Adhesive Stresses in Wide Flange Steel Beams Bonded To GFRP Plate under Transverse Bending. *International Conference on Civil, Structural and Transportation Engineering*, Ottawa, Ontario, Canada, May 4-5, 2015, pp 268-1 – 268-10.